Acta Crystallographica Section D
Biological Crystallography
ISSN 0907-4449

A novel crystal form of pyrrolysyl-tRNA synthetase reveals the pre- and post-aminoacyl-tRNA synthesis conformational states of the adenylate and aminoacyl moieties and an asparagine residue in the catalytic site

Tatsuo Yanagisawa,[a] Tomomi Sumida,[a] Ryohei Ishii[a] and Shigeyuki Yokoyama[a,b]*

[a]RIKEN Systems and Structural Biology Center, 1-7-22 Suehiro, Tsurumi, Yokohama 230-0045, Japan, and [b]Department of Biophysics and Biochemistry and Laboratory of Structural Biology, Graduate School of Science, The University of Tokyo, 7-3-1 Hongo, Bunkyo, Tokyo 113-0033, Japan

Correspondence e-mail: yokoyama@biochem.s.u-tokyo.ac.jp, yokoyama@riken.jp

Received 28 May 2012
Accepted 19 September 2012

PDB References: pyrrolysyl-tRNA synthetase complexes, 3vqw; 3vqx; 3vqy

Structures of *Methanosarcina mazei* pyrrolysyl-tRNA synthetase (PylRS) have been determined in a novel crystal form. The triclinic form crystals contained two PylRS dimers (four monomer molecules) in the asymmetric unit, in which the two subunits in one dimer each bind N^{ε}-(*tert*-butyloxycarbonyl)-L-lysyladenylate (BocLys-AMP) and the two subunits in the other dimer each bind AMP. The BocLys-AMP molecules adopt a curved conformation and the C^{α} position of BocLys-AMP protrudes from the active site. The $\beta7$–$\beta8$ hairpin structures in the four PylRS molecules represent distinct conformations of different states of the aminoacyl-tRNA synthesis reaction. Tyr384, at the tip of the $\beta7$–$\beta8$ hairpin, moves from the edge to the inside of the active-site pocket and adopts multiple conformations in each state. Furthermore, a new crystal structure of the BocLys–AMPPNP-bound form is also reported. The bound BocLys adopts an unusually bent conformation, which differs from the previously reported structure. It is suggested that the present BocLys–AMPPNP-bound, BocLys-AMP-bound and AMP-bound complexes represent the initial binding of an amino acid (or pre-aminoacyl-AMP synthesis), pre-aminoacyl-tRNA synthesis and post-aminoacyl-tRNA synthesis states, respectively. The conformational changes of Asn346 that accompany the aminoacyl-tRNA synthesis reaction have been captured by X-ray crystallographic analyses. The orientation of the Asn346 side chain, which hydrogen-bonds to the carbonyl group of the amino-acid substrate, shifts by a maximum of 85–90° around the C^{β} atom.

1. Introduction

In protein synthesis, the universal genetic code is established in a single biochemical reaction: the aminoacylation of tRNA. Aminoacyl-tRNAs corresponding to the 20 canonical amino acids are generated by the ligation of the encoded amino acid to its cognate tRNAs by specific aminoacyl-tRNA synthetases (aaRSs; Schimmel, 1987; Ibba & Söll, 2000). The aaRSs catalyze a two-step reaction involving condensation of the amino acid with ATP to yield the aminoacyladenylate (aminoacyl-AMP) intermediate followed by transfer of the amino acid to the 3′-terminal adenosine of the tRNA. The aaRSs have been divided into two distinct classes of ten enzymes each, the class I and class II aaRSs, which are unrelated in both sequence and structure (Eriani *et al.*, 1990). The catalytic domain of the class I aaRSs is formed by the so-called Rossmann-fold nucleotide-binding domain, while the class II enzymes have catalytic domains organized around

© 2013 International Union of Crystallography
Printed in Singapore – all rights reserved

Table 1
PylRS crystal structures.

Name	Constituents	Resolution (Å)	PDB entry	References
PylRS(c270)	Catalytic fragment of *M. mazei* pyrrolysyl-tRNA synthetase, ligand-free form	2.65	2e3c	Yanagisawa *et al.* (2008*a*)
PylRS(c270)–AMPPNP	Catalytic fragment of *M. mazei* pyrrolysyl-tRNA synthetase and adenosine 5′-(β,γ-imido)triphosphate	1.8	2q7e	Kavran *et al.* (2007)
PylRS(c270)–AMPPNP	Catalytic fragment of *M. mazei* pyrrolysyl-tRNA synthetase and adenosine 5′-(β,γ-imido)triphosphate	1.9	2zcd, 3vqv	Yanagisawa *et al.* (2008*a*)
PylRS(c270)(SeMet)–AMPPNP	Catalytic fragment of *M. mazei* pyrrolysyl-tRNA synthetase (selenomethione-substituted) and adenosine 5′-(β,γ-imido)triphosphate	2.4	3vqw	Yanagisawa *et al.* (2008*a*)
PylRS(c270)–BocLys–AMPPNP (initial state of an amino-acid binding or pre-aminoacyl-AMP synthesis) (form 2)	Catalytic fragment of *M. mazei* pyrrolysyl-tRNA synthetase, N^{ε}-(*tert*-butyloxycarbonyl)-L-lysine and adenosine 5′-(β,γ-imido)triphosphate	2.4	3vqy	This study
PylRS(c270)–Pyl–AMPPNP	Catalytic fragment of *M. mazei* pyrrolysyl-tRNA synthetase, pyrrolysine and adenosine 5′-(β,γ-imido)triphosphate	1.8	2zce	Yanagisawa *et al.* (2008*a*)
PylRS(c270)–BocLys–AMPPNP (form 1)	Catalytic fragment of *M. mazei* pyrrolysyl-tRNA synthetase, N^{ε}-(*tert*-butyloxycarbonyl)-L-lysine and adenosine 5′-(β,γ-imido)triphosphate	1.79	2zin	Yanagisawa *et al.* (2008*b*)
PylRS(c270)–CpocLys–ATP	Catalytic fragment of *M. mazei* pyrrolysyl-tRNA synthetase, N^{ε}-cyclopentyloxycarbonyl-D-lysine and ATP	1.9	2q7g	Kavran *et al.* (2007)
PylRS(c270)–Pyl-AMP–PP_i	Catalytic fragment of *M. mazei* pyrrolysyl-tRNA synthetase and pyrrolysyladenylate	2.1	2zim	Kavran *et al.* (2007)
PylRS(c270)–AlocLys-AMP–PNP	Catalytic fragment of *M. mazei* pyrrolysyl-tRNA synthetase, N^{ε}-allyloxycarbonyl-L-lysyladenylate and PNP pyrophosphate	2.06	2zio	Yanagisawa *et al.* (2008*b*)
PylRS(c270)–BocLys-AMP (pre-aminoacyl-tRNA synthesis)	Catalytic fragment of *M. mazei* pyrrolysyl-tRNA synthetase and N^{ε}-(*tert*-butyloxycarbonyl)-L-lysyladenylate	2.3	3vqx	This study
PylRS(c270)–AMP (post-aminoacyl-tRNA synthesis)	Catalytic fragment of *M. mazei* pyrrolysyl-tRNA synthetase and adenosine 5′-monophosphate	2.3	3vqx	This study
oMeTyrRS–oMeTyr–AMPPNP	Catalytic fragment of *M. mazei* pyrrolysyl-tRNA synthetase mutant A302T/N346V/C348W/Y384F/V401L, *o*-methyl-L-tyrosine and adenosine 5′-(β,γ-imido)triphosphate	1.75	3qtc	Takimoto *et al.* (2011)
*Dh*PylRS	*D. hafniense* pyrrolysyl-tRNA synthetase, ligand-free form	2.1	3dsq	Lee *et al.* (2008)
*Dh*PylRS	*D. hafniense* pyrrolysyl-tRNA synthetase, ligand-free form	2.5	2znj	Nozawa *et al.* (2009)
*Dh*PylRS–$tRNA^{Pyl}$	*D. hafniense* pyrrolysyl-tRNA synthetase and $tRNA^{Pyl}$	3.1	2zni	Nozawa *et al.* (2009)

a seven-stranded antiparallel β-sheet and are characterized by three conserved motifs: motif 1, motif 2 and motif 3 (Cusack *et al.*, 1990; Ruff *et al.*, 1991). To date, structures of all known class II aaRSs have been solved and the structural bases of substrate recognition have been determined. In general, the class II enzymes form dimers or tetramers (Ibba & Söll, 2000) and contain mobile active-site loops, including the motif 2 loop (Cavarelli *et al.*, 1994; Belrhali *et al.*, 1994), the ordering loop (Yaremchuk *et al.*, 2001; Torres-Larios *et al.*, 2003), which is also termed the flipping loop (Schmitt *et al.*, 1998; Eiler *et al.*, 1999) or the helical loop (Moor *et al.*, 2006), and the cognate amino-acid loop [*e.g.* histidyl-tRNA synthetase (HisRS; Arnez *et al.*, 1995; Aberg *et al.*, 1997; Yaremchuk *et al.*, 2001), prolyl-tRNA synthetase (ProRS; Yaremchuk *et al.*, 2001), threonyl-tRNA synthetase (ThrRS; Torres-Larios *et al.*, 2003; Bovee *et al.*, 2003), seryl-tRNA synthetase (SerRS; Bilokapic *et al.*, 2006) and glycyl-tRNA synthetase (GlyRS; Arnez *et al.*, 1999)], which in many cases undergo conformational changes that are induced upon substrate binding.

Pyrrolysyl-tRNA synthetase (PylRS), one of the class II aaRSs, catalyzes the ligation of pyrrolysine (Pyl) to its cognate tRNA ($tRNA^{Pyl}$; Srinivasan *et al.*, 2002; Hao *et al.*, 2002; Blight *et al.*, 2004; Polycarpo *et al.*, 2004). Crystal structures of the catalytic fragment of *Methanosarcina mazei* PylRS in complex with various substrates have been solved (Yanagisawa *et al.*, 2006, 2008*a*,*b*; Kavran *et al.*, 2007; Takimoto *et al.*, 2011; Table 1). These studies included *M. mazei* PylRS structures complexed with AMPPNP (Kavran *et al.*, 2007; Yanagisawa *et al.*, 2008*a*), Pyl-AMP–PP_i (Kavran *et al.*, 2007), N^{ε}-cyclopentyloxycarbonyl-D-lysine (CpocLys)–ATP (Kavran *et al.*, 2007), Pyl–AMPPNP (Yanagisawa *et al.*, 2008*a*), N^{ε}-(*tert*-butyloxycarbonyl)-L-lysine (BocLys)–AMPPNP (Yanagisawa *et al.*, 2008*b*), N^{ε}-allyloxycarbonyl-L-lysyladenylate (AlocLys-AMP)–PNP (Yanagisawa *et al.*, 2008*b*), *o*-methyl-L-tyrosine (oMeTyr)–AMPPNP (Takimoto *et al.*, 2011) and the ligand-free form (Yanagisawa *et al.*, 2008*a*). Furthermore, the ligand-free and $tRNA^{Pyl}$ complex structures of *Desulfitobacterium hafniense* PylRS have been solved (Lee *et al.*, 2008; Nozawa *et al.*, 2009). Like the other class II aaRSs, PylRS exists as a dimer and has three active-site loops. A comparison of these structures revealed conformational diversity of the motif 2 loop, the ordering loop and the $\beta7$–$\beta8$ hairpin, which corresponds to the cognate amino-acid loop in the class II aaRSs (Yanagisawa *et al.*, 2008*a*). The motif 2 and ordering loops close upon binding ATP (or its analogue) or Pyl-AMP, and the $\beta7$–$\beta8$ hairpin undergoes multiple conformational transitions between open, intermediate and closed states regardless of the bound substrates (Yanagisawa *et al.*, 2008*a*).

Here, we report the structures of PylRS in new BocLys–AMPPNP-bound, BocLys-AMP-bound and AMP-bound

Table 2
Data-collection and refinement statistics.

Values in parentheses are for the last shell.

	PylRS(c270) triclinic form	PylRS(c270)–BocLys–AMPPNP
PDB code	3vqx	3vqy
X-ray source	BL41XU, SPring-8	AR-NW12, Photon Factory
Wavelength (Å)	1.0000	1.0000
Space group	$P1$	$P6_4$
Unit-cell parameters (Å, °)	a = 62.80, b = 69.42, c = 83.33, α = 106.9, β = 91.4, γ = 113.8	$a = b$ = 103.36, c = 70.91, $\alpha = \beta$ = 90, γ = 120
Resolution (Å)	50–2.3 (2.34–2.30)	50–2.4 (2.44–2.40)
$\langle I/\sigma(I)\rangle$	14.0 (2.14)	23.8 (2.36)
Completeness (%)	83.9 (64.3)	97.2 (92.5)
No. of reflections	45275	16537
Multiplicity (%)	1.6	6.7
$R_{\rm merge}$†	3.7 (21.9)	7.9 (24.7)
Refinement		
$R_{\rm work}$‡/$R_{\rm free}$§ (%)	21.3/27.0	19.7/23.1
Resolution (Å)	50–2.3	50–2.4
No. of atoms		
Protein	8236	2087
Others	144	50
Water	164	98
No. of reflections (work/test)	40705/4573	14869/1661
Average B factors (Å^2)		
Protein	46.0	45.3
Ligands	64.1	53.3
Water	42.1	50.2
R.m.s. deviations		
Bond lengths (Å)	0.007	0.007
Bond angles (°)	1.5	1.4
Ramachandran plot		
Most favoured (%)	90.6	93.7
Allowed (%)	9.3	6.3
Disallowed (%)	0.1	0.0

† $R_{\rm merge} = \sum_{hkl}\sum_i |I_i(hkl) - \langle I(hkl)\rangle|/\sum_{hkl}\sum_i I_i(hkl)$. ‡ $R_{\rm work} = \sum_{hkl} ||F_{\rm obs}| - |F_{\rm calc}||/\sum_{hkl}|F_{\rm obs}|$ for reflections in the work set. § $R_{\rm free} = \sum_{hkl} ||F_{\rm obs}| - |F_{\rm calc}||/\sum_{hkl}|F_{\rm obs}|$ for reflections in the test set [10% of the total reflections for *M. mazei* PylRS(c270)].

forms. On the basis of the present and previous PylRS structures, we discuss the conformational states of the bound adenylate and aminoacyl moieties and the Asn side chain in the catalytic site, along with the aminoacylation reaction.

2. Materials and methods

2.1. tRNA preparation, protein purification and crystallization

M. mazei tRNA$^{\rm Pyl}$ was transcribed *in vitro* with T7 RNA polymerase and purified by Resource Q column chromatography (GE Healthcare). The native catalytic fragment of *M. mazei* PylRS [PylRS(c270)] was purified as described by Yanagisawa *et al.* (2006). Initial crystallization-condition screening was conducted using commercially available crystallization screening kits from Hampton Research, Emerald BioStructures and Molecular Dimensions. We cocrystallized PylRS(c270) (3.6 mg ml^{-1}, 107 µ*M*) with tRNA$^{\rm Pyl}$ (2.7 mg ml^{-1}, 129 µ*M*), BocLys (1.7 m*M*) and AMPPNP (5 m*M*) and obtained plate-like crystals at 293 K in 2 d using the hanging-drop vapour-diffusion method in 100 m*M* sodium cacodylate buffer pH 6.8 containing 0.2 *M* sodium/potassium tartrate and 2 *M* ammonium sulfate. For cryoprotection, the crystals were briefly soaked in reservoir solution containing 15% glycerol. BocLys–AMPPNP-bound PylRS(c270) crystals were obtained by the hanging-drop vapour-diffusion method in 100 m*M* sodium cacodylate buffer pH 7.0 containing 10 m*M* $MgCl_2$, 5% PEG 3350, 5 m*M* BocLys, 5 m*M* AMPPNP (Yanagisawa *et al.*, 2006, 2008*a*). For cryoprotection, the crystals were briefly soaked in reservoir solution containing 35% glycerol.

2.2. Data collection and processing

A 2.3 Å resolution data set was collected from cryocooled (100 K) triclinic crystals of the AMP-bound (and BocLys-AMP-bound) form on beamline BL41XU at SPring-8. A 2.4 Å resolution data set was collected from hexagonal crystals of the BocLys–AMPPNP-bound form on beamline AR-NW12 at the Photon Factory. Data-collection statistics are summarized in Table 1. The PylRS(c270) crystal belonged to the triclinic space group $P1$, with unit-cell parameters a = 62.8, b = 69.42, c = 83.33 Å, α = 106.92, β = 91.41, γ = 113.83°; the asymmetric unit contained four PylRS(c270) molecules, with a corresponding crystal volume per protein weight ($V_{\rm M}$) of 2.36 Å^3 Da^{-1} and a solvent content of 48%. All data were processed using the *HKL*-2000 program suite (Otwinowski & Minor, 1997); other crystallographic calculations were performed using the *CCP*4 package (Winn *et al.*, 2011).

2.3. Structure determination and refinement

The structures of AMP-bound (and BocLys-AMP-bound) PylRS(c270) and of BocLys–AMPPNP-bound PylRS(c270) were solved by the molecular-replacement method using the structure of selenomethionine-substituted PylRS(c270) bound to AMPPNP (PDB entry 3vqw; Yanagisawa *et al.*, 2008*a*) as the search model. Model building was accomplished with *O* (Jones *et al.*, 1991), *CueMol* (http://cuemol.sourceforge.jp/en/) and *Coot* (Emsley & Cowtan, 2004) and refinement was performed using *CNS* (Brünger *et al.*, 1998) and *REFMAC*5 (Murshudov *et al.*, 2011). The quality of the model was analyzed with *PROCHECK* (Winn *et al.*, 2011). Graphical images were prepared with the programs *CueMol*, *PyMOL* (http://www.pymol.org) and *POV-Ray* (http://www.povray.org/). The data-collection and refinement statistics are summarized in Table 2. Superpositions of the C$^\alpha$ traces of the PylRS(c270) structures were produced using the *Secondary Structure Matching* (*SSM*) program (Krissinel & Henrick, 2004).

2.4. Data deposition

Atomic coordinates and structure factors for the *M. mazei* PylRS(c270)–AMP (and BocLys-AMP), PylRS(c270)–BocLys–AMPPNP and selenomethionine-substituted PylRS(c270)–AMPPNP complexes have been deposited in the Protein Data Bank (PDB entries 3vqx, 3vqy and 3vqw, respectively).

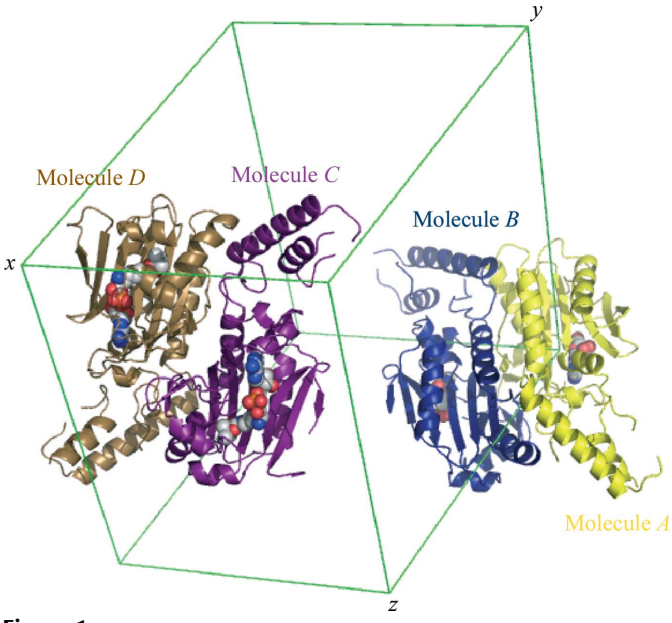

Figure 1
Crystal packing of a triclinic-form crystal of *M. mazei* PylRS(c270). The two subunits that form a biologically active homodimer are shown in different colours. AMP and BocLys-AMP are shown as sphere models. The unit cells are also shown.

3. Results

3.1. Overall structures

We determined the crystal structure of the catalytic fragment of *M. mazei* PylRS [PylRS(c270)] complexed with AMP (and BocLys-AMP) at 2.3 Å resolution with final R and $R_{\rm free}$ factors of 21.3% and 27.0%, respectively (Table 2). The triclinic crystals contained two homodimers (*AB* and *CD*) in the asymmetric unit, which comprised 255, 243, 257 and 257 residues with visible density (residues 191–208, 212–279 and 286–454 for molecule *A*; residues 188–208, 213–279, 287–332, 334–377 and 387–454 for molecule *B*; residues 190–207, 212–281, 284–378 and 381–454 for molecule *C*; residues 191–207, 210–279, 283–332 and 335–454 for molecule *D*; Fig. 1). The present PylRS(c270) structures are essentially similar to the previously reported PylRS(c270) structures in the hexagonal form (236–241 PylRS residues with an r.m.s.d. of 0.64–0.84 Å for the C^{α} atoms). Furthermore, we determined a new crystal structure of PylRS(c270)–BocLys–AMPPNP at 2.4 Å resolution using hexagonal-form crystals grown under the previously reported conditions (Yanagisawa *et al.*, 2006). The final R and $R_{\rm free}$ factors refined to 19.7% and 23.1%, respectively (Table 2). As expected, the overall structure was the same as

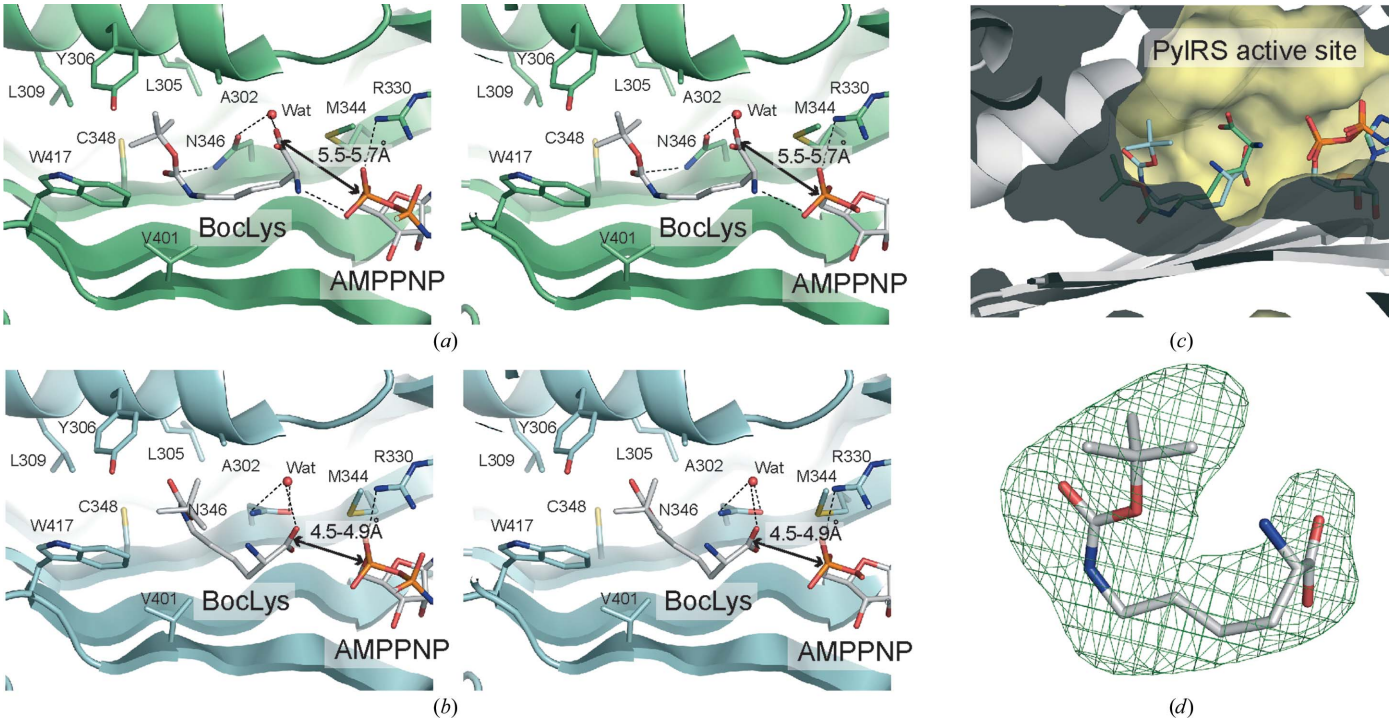

Figure 2
Crystal structures of BocLys bound to PylRS. (*a*, *b*) Stereoviews of the previously determined form 1 (*a*) and the present form 2 (*b*) structures of BocLys–AMPPNP-bound PylRS(c270). (*c*) Superposition of the form 1 (blue white) and form 2 (light green) structures. (*d*) The $F_{\rm o} - F_{\rm c}$ OMIT electron-density map (contoured at 4σ) of the unusually bent enzyme-bound BocLys in form 2.

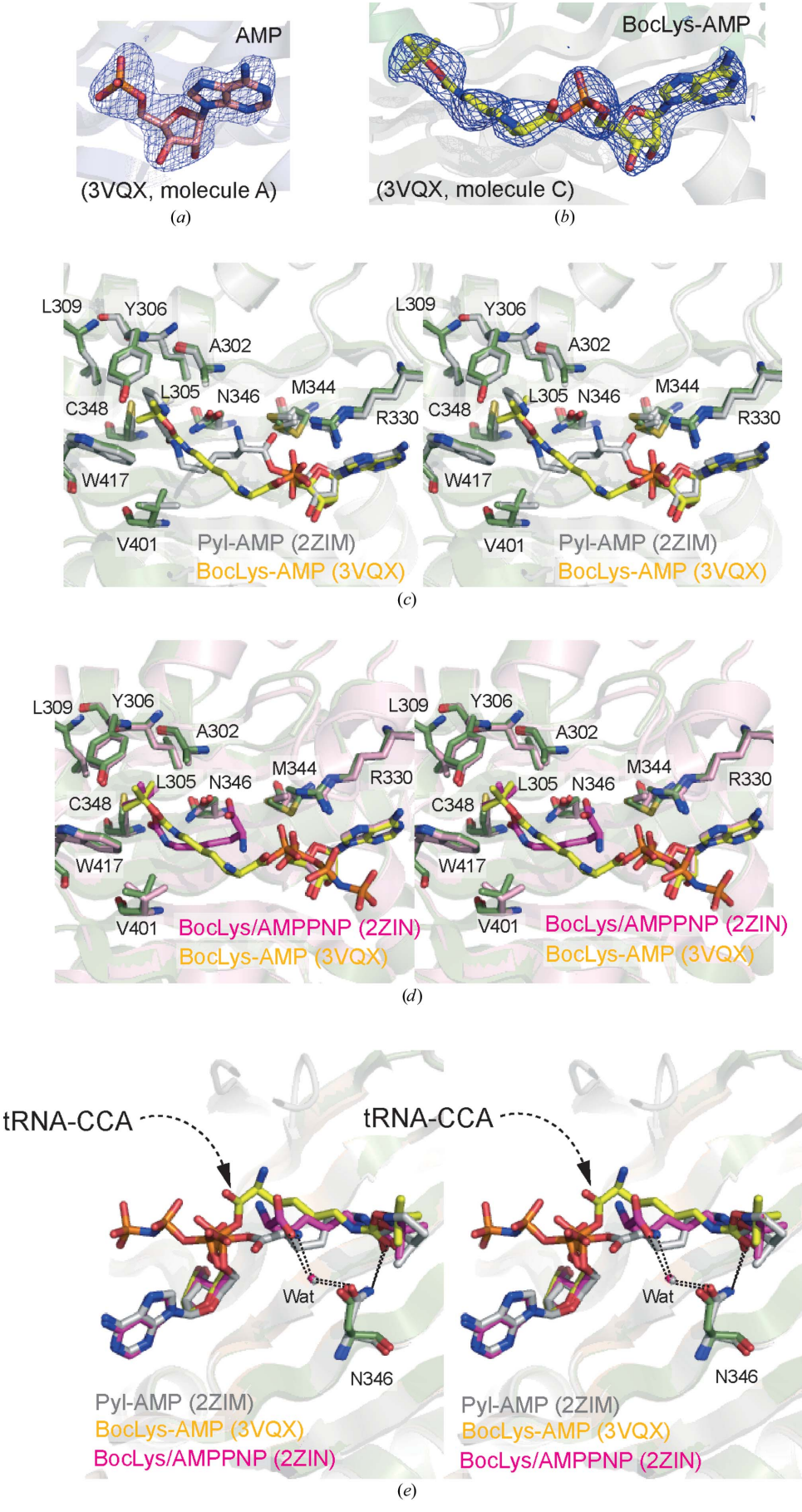

that of previously reported PylRS(c270) structures (Kavran *et al.*, 2007; Yanagisawa *et al.*, 2008*a*,*b*).

3.2. The structure of PylRS in the BocLys-bound form

Although the PylRS(c270) structures in the two crystal forms were essentially the same (Figs. 2*a* and 2*b*), the structures of the bound BocLys differed significantly from each other (Yanagisawa *et al.*, 2008*b*). The *tert*-butyloxycarbonyl (Boc) group in the present BocLys-bound form (form 2) points outwards from the hydrophobic pocket, while the *tert*-butyl (*t*Bu) moiety of BocLys in the previous BocLys-bound PylRS(c270) structure (form 1) was accommodated within the hydrophobic pocket in the same manner as Pyl (Kavran *et al.*, 2007; Yanagisawa *et al.*, 2008*a*), AlocLys (Yanagisawa *et al.*, 2008*b*) and CpocLys (Kavran *et al.*, 2007) (Fig. 2*c*). The structures of the amino-acid side chains forming the hydrophobic pocket in the PylRS active site are the same in both crystal forms. In contrast, the positions of the side-chain amide of Asn346 are different. The Asn346 side

Figure 3
Crystal structures of AMP and BocLys-AMP bound to PylRS. (*a*, *b*) The $F_o - F_c$ OMIT electron-density maps (contoured at 4σ) of the bound AMP (PDB entry 3vqx, molecule *A*) (*a*) and BocLys-AMP (PDB entry 3vqx, molecule *C*) (*b*) are represented as ball-and-stick models. Transparent ribbon models of the AMP-bound (and BocLys-AMP-bound) forms are visible in the background. (*c*) Superposition of the structures of the previously determined form 1 (white) and BocLys-AMP-bound (grass green) forms. (*d*) Superposition of the structures of the Pyl-AMP-bound (white) and BocLys-AMP-bound forms (grass green). (*e*) The Asn346 side chain hydrogen-bonds to the carbonyl group of the amino-acid substrate and a water-mediated hydrogen bond exists between the α-carboxyl group of BocLys (or the α-amino group of pyrrolysyl-AMP) and the side-chain amide group of Asn346.

chain points toward the α-phosphate group of AMPPNP in the present structure, whereas it hydrogen-bonds to the N^{ε}-carbonyl group of BocLys in form 1 (Figs. 2*a* and 2*b*; Yanagisawa *et al.*, 2008*b*). Note that conformational changes of Asn346 upon substrate binding were also observed upon binding with other substrates, as discussed below. There are no large hydrophobic interactions between the *t*Bu moiety and the PylRS active site (Fig. 2*c*). Consequently, the electron density of the bound BocLys in form 2 was weaker than that of the bound BocLys in form 1, implying that the present BocLys structure is less stable than the previously reported structure (Fig. 2*d*). On the other hand, the distances between the α-carboxylate of BocLys and the α-phosphate of AMPPNP in form 2 (4.5–4.9 Å) are shorter than those in form 1 (5.5–5.7 Å) (Figs. 2*a* and 2*b*).

3.3. The structure of PylRS in the AMP-bound and BocLys-AMP-bound form

Electron density corresponding to bound AMP was observed in molecules *A* and *B* (Fig. 3*a*) and that corresponding to bound BocLys-AMP was observed in molecules *C* and *D* (Fig. 3*b*) in the triclinic-form crystal. Although the crystallization experiments were performed in the presence of PylRS(c270), BocLys, AMPPNP and $tRNA^{Pyl}$, no electron density was observed for either the tRNA molecule or AMPPNP. Therefore, we assumed that the reaction producing BocLys-AMP and AMP occurred spontaneously during the experiment. In the BocLys-AMP-bound form and form 1, the Boc and AMP moieties, together with their surrounding PylRS side chains, are located in the same positions (Fig. 3*c* and 3*d*). The side-chain amide group of Asn346 hydrogen-bonds to the N^{ε}-carbonyl group of the amino-acid substrate, as observed in form 1 (Fig. 3*e*). However, there are two major differences between these structures. Firstly, the Boc group of BocLys-AMP tilts and the carbonyl group moves towards Asn346, which maintains the same position in both structures. Secondly, the α-carboxyl group of BocLys-AMP is flipped out toward the phosphate group, so that the aminoacyl-AMP molecule is formed without movement of the ATP molecule (Figs. 3*d* and 3*e*). In the BocLys-AMP-bound structure no water-mediated interaction exists between BocLys-AMP and the side-chain amide group of Asn346. On the other hand, in form 1 and the pyrrolysyl-AMP-bound form there is a water-mediated interaction between the α-carboxyl group of BocLys (or the α-amino group of pyrrolysyl-AMP) and the side-chain

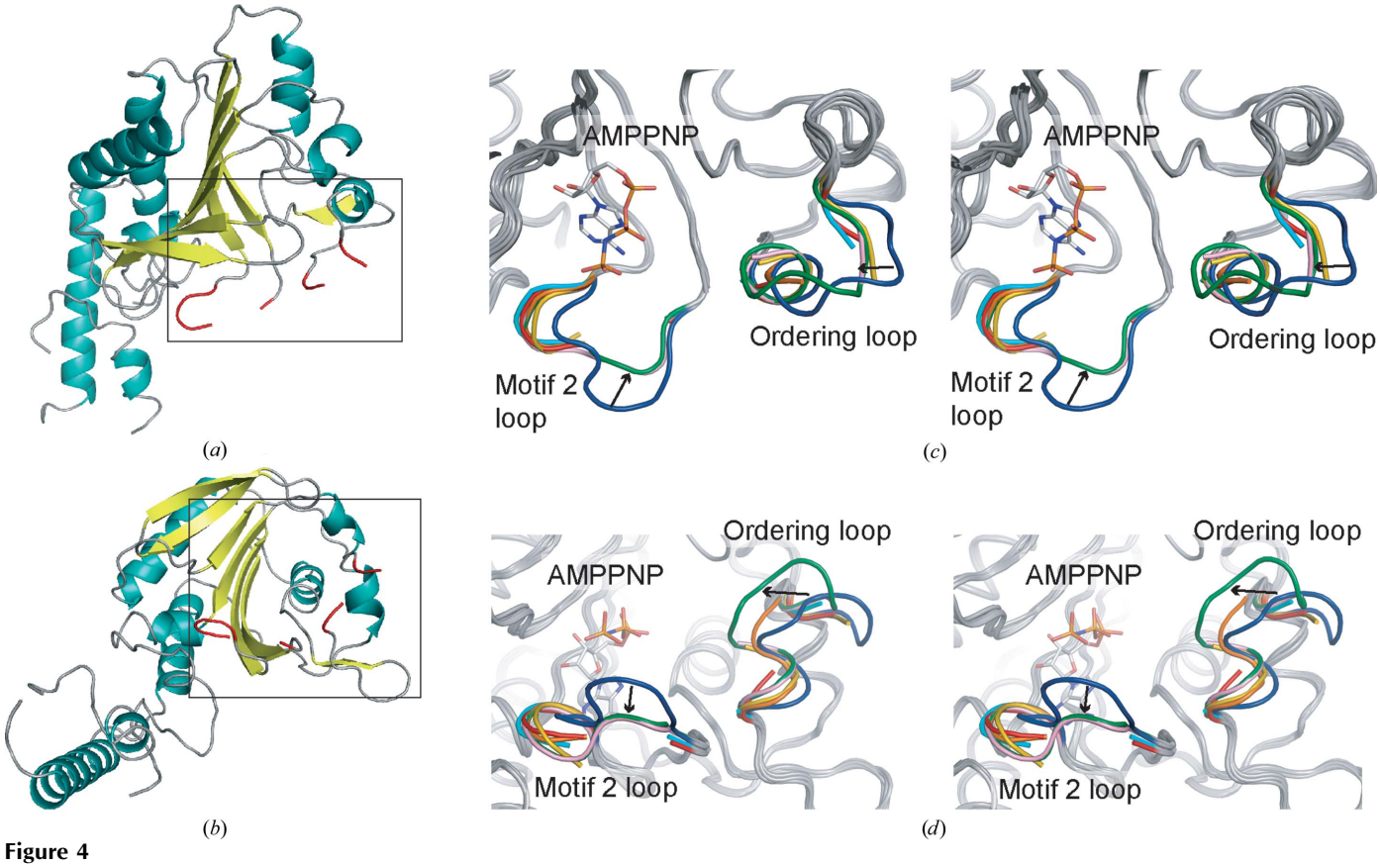

Figure 4
Conformational changes of the motif 2 loop and the ordering loop. (*a*, *b*) Overall structures of the triclinic crystal form of PylRS(c270) (PDB entry 3vqx, molecule *A*). The motif 2 and ordering loops are coloured red. (*c*, *d*) Close-up stereoviews of motif 2 and the ordering loops (boxed regions in *a* and *b*). The superpositioned C^{α} traces of the AMP-bound (red and cyan traces; residues 277–286 and 331–337) and BocLys-AMP-bound forms (yellow and orange traces; residues 277–286 and 331–337) with those of the ligand-free (dark blue trace; residues 277–286 and 331–337; PDB entry 2e3c) and two AMPPNP-bound forms (green and pink traces; residues 277–286 and 331–337; PDB entries 2zcd and 2q7e) are shown. Arrows indicate the open-to-closed conformations of the motif 2 and ordering loops.

amide group of Asn346. The rotation of the α-carboxyl group causes the aminoacyl-AMP to adopt an unusual conformation (Figs. 3*d* and 3*e*). In general, the dihedral angle of an aminoacyl-AMP involving the C, O, P and O5′ atoms ranges from −40° to −110°, while those of BocLys-AMP are 127° and 153° for molecules *C* and *D*, respectively (Fig. 3*e*).

3.4. The motif 2 and ordering loops

The structural differences between the ligand-free form, the AMPPNP-bound form, the present AMP-bound (and BocLys-AMP-bound) form, form 1 and form 2 are mainly limited to the ordering loop, the motif 2 loop (Fig. 4) and the β7–β8 hairpin (Fig. 5). ATP binding causes conformational changes in the ordering and motif 2 loops, which revealed that PylRS uses a different subset of the possible induced-fit mechanisms observed for other class II aaRSs (Yanagisawa *et al.*, 2008*a*). The structures of the ordering and motif 2 loops in the present AMP-bound (and BocLys-AMP-bound) and BocLys–AMPPNP-bound structures resemble those of the AMPPNP-bound form rather than the ligand-free form, although the electron density was weaker and some residues in the loop were excluded from the model (Figs. 4*a* and 4*b*). These results indicated that the conformational changes induced upon ATP binding are not influenced by either amino-acid binding or ATP hydrolysis.

3.5. The β7–β8 hairpin

We found that the β-hairpins (residues 375–392) between β7 and β8 adopt quite distinct conformations in each of the four PylRS(c270) molecules in the triclinic-form crystals. The β-hairpins are located in different regions from the edge of the antiparallel β-sheet to the inside of the active-site pocket (Figs. 5*a* and 5*b*). The entire structures of the hairpins are well ordered in molecules *A* and *D*, while some parts of the hairpins are disordered in molecules *B* (residues Asp379–Thr387) and *C* (residues Asp379 and Ser380). In molecules *B*, *C* and *D* the β7–β8 hairpin assumes a straight structure that extends to the tip (Fig. 5*b*). In contrast, in molecule *A* the β7–β8 hairpin is bent around Gly378/Asp379 (β7) and Gly385/Asp386 (β8) and half of the β-hairpin is turned towards the active site, although the bending angle is smaller than those in the AMPPNP-bound and Pyl-AMP-bound forms reported by Kavran *et al.* (2007) (Fig. 5*c*). Note that the β7–β8 hairpins of molecules *A* and *D* interact with each other by crystal packing, which stabilizes the hairpin conformation. This may be one of the reasons why the β7–β8 hairpins in each subunit adopt

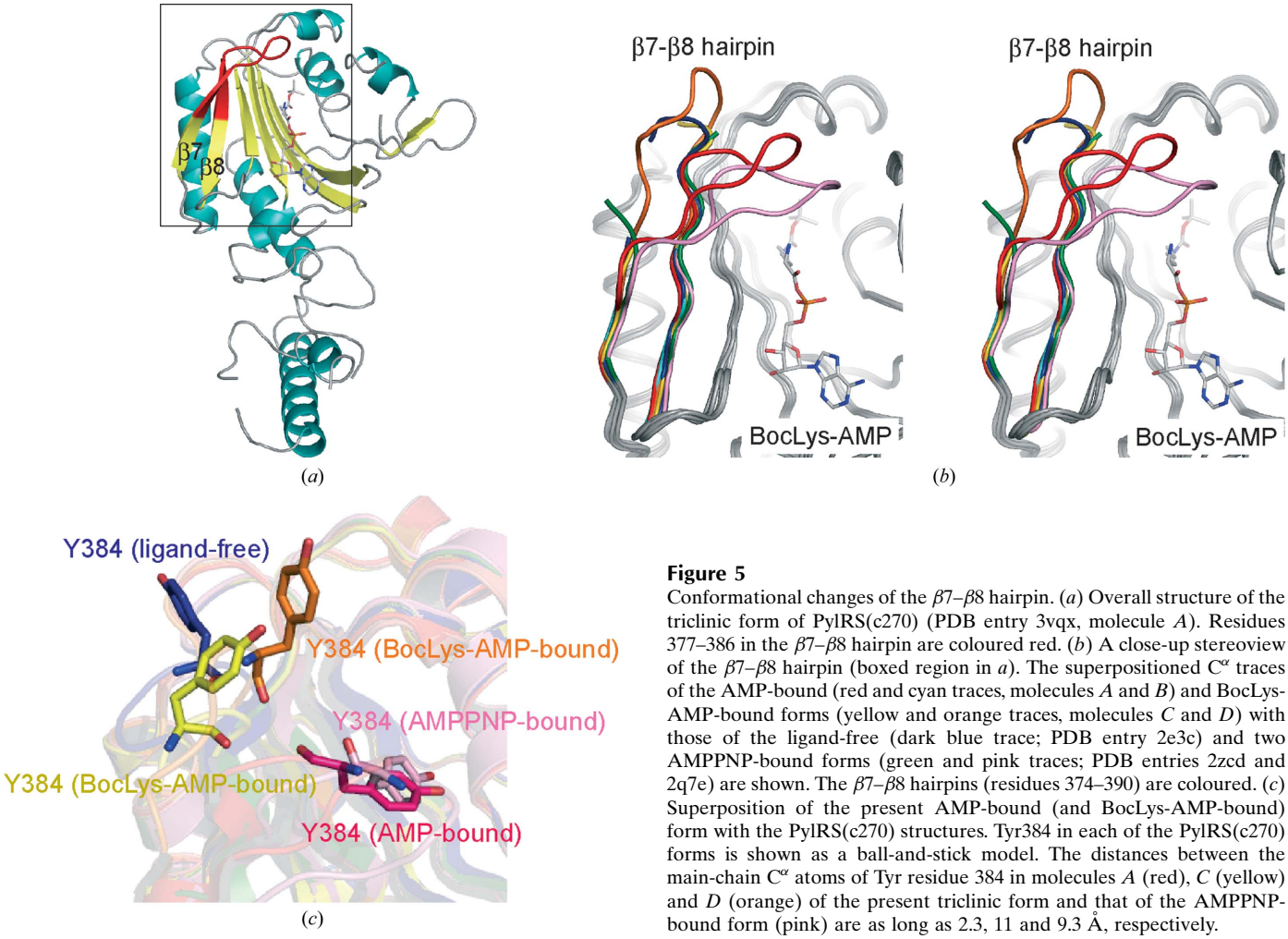

Figure 5
Conformational changes of the β7–β8 hairpin. (*a*) Overall structure of the triclinic form of PylRS(c270) (PDB entry 3vqx, molecule *A*). Residues 377–386 in the β7–β8 hairpin are coloured red. (*b*) A close-up stereoview of the β7–β8 hairpin (boxed region in *a*). The superpositioned C$^{\alpha}$ traces of the AMP-bound (red and cyan traces, molecules *A* and *B*) and BocLys-AMP-bound forms (yellow and orange traces, molecules *C* and *D*) with those of the ligand-free (dark blue trace; PDB entry 2e3c) and two AMPPNP-bound forms (green and pink traces; PDB entries 2zcd and 2q7e) are shown. The β7–β8 hairpins (residues 374–390) are coloured. (*c*) Superposition of the present AMP-bound (and BocLys-AMP-bound) form with the PylRS(c270) structures. Tyr384 in each of the PylRS(c270) forms is shown as a ball-and-stick model. The distances between the main-chain C$^{\alpha}$ atoms of Tyr residue 384 in molecules *A* (red), *C* (yellow) and *D* (orange) of the present triclinic form and that of the AMPPNP-bound form (pink) are as long as 2.3, 11 and 9.3 Å, respectively.

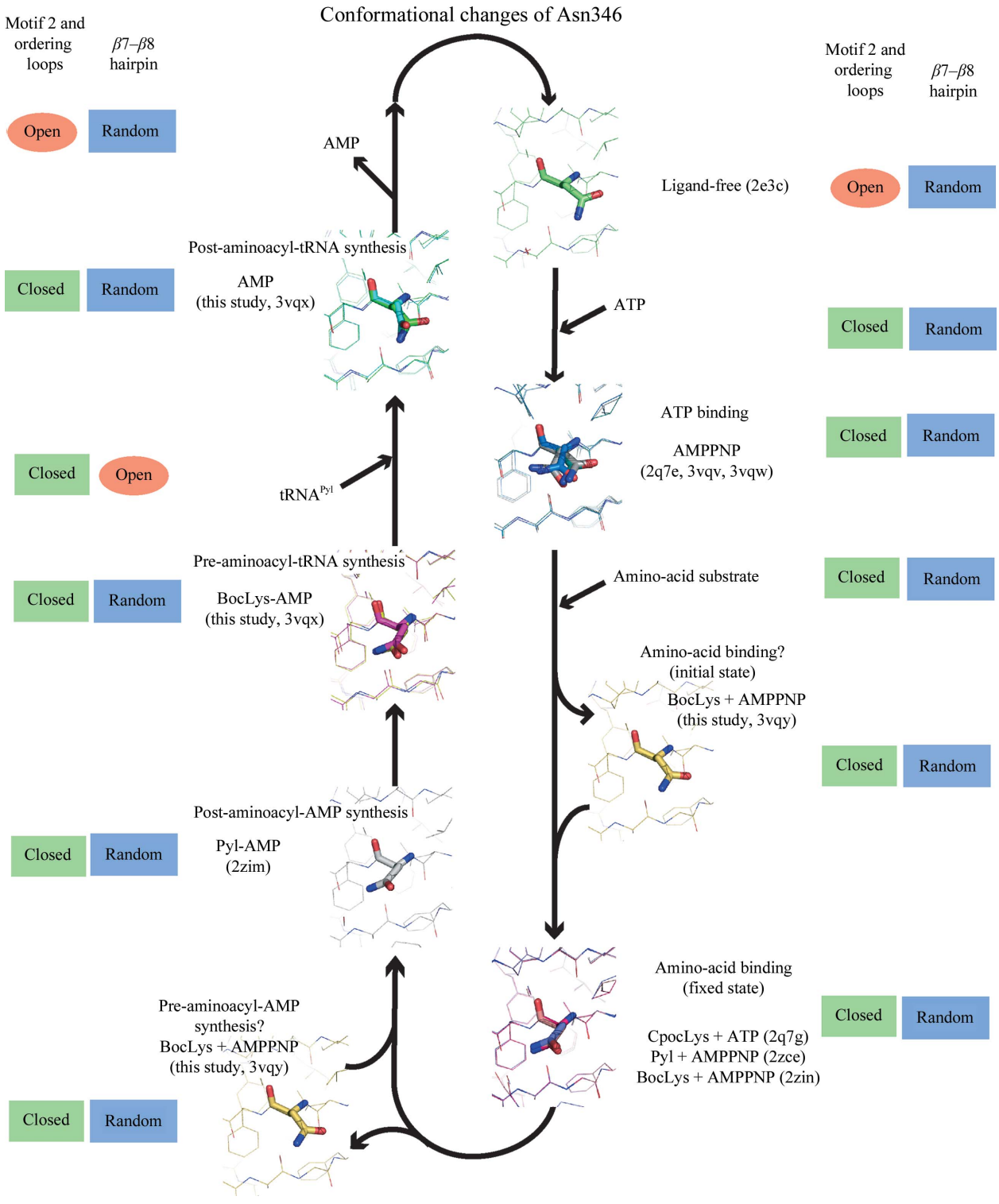

Figure 6
Snapshots of the Asn346 side chain during aminoacyl-tRNA synthesis. Schematic representation of the conformational changes of the Asn346 side chain according to the status of the tRNA-aminoacylation reaction. In the ATP-binding step (the AMPPNP-bound forms; PDB entries 2q7e, 3vqv and 3vqw), the Asn346 side chain fluctuates by approximately 60°. In the initial state of amino-acid binding or pre-aminoacyl-AMP synthesis (form 2; PDB entry 3vqy), the Asn346 side chain points toward the α-phosphate of AMPPNP and does not interact with the N^{ε}-carbonyl group of the amino-acid substrate. On the other hand, in the fixed state of amino-acid binding [CpocLys–ATP-bound form (PDB entry 2q7g), Pyl–AMPPNP-bound form (PDB entry 2zce) and form 1 (PDB entry 2zin)], the Asn346 side chain interacts specifically with the N^{ε}-carbonyl group of the bound amino-acid substrate. The specific interactions between the Asn346 side chain and the N^{ε}-carbonyl group of the amino-acid substrate remain unchanged during aminoacyl-AMP synthesis [Pyl-AMP-bound form (PDB entry 2zim) and BocLys-AMP-bound form (PDB entry 3vqx)]. The orientation of the Asn346 side chain shifts by a maximum of 85–90° around the C^{β} atom, compared with that in the post-aminoacyl-AMP synthesis state and the fixed state of amino-acid binding, after the aminoacyl-tRNA synthesis (AMP-bound form; PDB entry 3vqx) and following AMP release (ligand-free form; PDB entry 2e3c). The conformations of motif 2, the ordering loops and the β7–β8 hairpin along with the aminoacylation reaction are also shown.

different conformations even though they are bound to the same substrate. The ordering of the $\beta7$–$\beta8$ hairpin in the interactions between molecules *A* and *D* leads to almost no difference within the active site of molecule *A* compared with molecule *B* or that of molecule *C* compared with molecule *D*. The Tyr384 residues at the tip of the $\beta7$–$\beta8$ hairpins in both BocLys-AMP-bound forms are located far from the active site. On the other hand, one of the two Tyr384 residues in the AMP-bound form was inside the active-site pocket, whereas the other was disordered (Fig. 5*c*). These results confirmed that the $\beta7$–$\beta8$ hairpin is very flexible, regardless of substrate binding, as described previously (Yanagisawa *et al.*, 2008*a*).

4. Discussion

There are two possible explanations for the conformational states of the present form 2 structure. The BocLys molecule in this structure is mobile (average *B* factor 89.1 Å^2), indicating that the structure represents the initial state of amino-acid binding (Fig. 2*c*). In the previously determined form 1 structure the bound BocLys is in a more ordered state and has a lower average *B* factor (56.4 Å^2), which might represent the fixed state of amino-acid binding to the PylRS active site (Yanagisawa *et al.*, 2008*b*). Another possibility is that the BocLys–AMPPNP-bound PylRS may exist in equilibrium between two different conformational states orresponding to forms 1 and 2. The bound BocLys in the present form 2 structure appears to be more reactive than that in the previously determined form 1 structure because the α-carboxyl group of BocLys is closer to the α-phosphate group of AMPPNP in form 1 than in form 2 (Figs. 2*a* and 2*b*).

Next, the bound BocLys-AMP in the triclinic crystal form is unusually bent, with its α-carboxyl group flipped outwards from the active site and thus susceptible to attack by the terminal adenosine of tRNA (Fig. 3*e*). We suggest that the present BocLys-AMP-bound PylRS structures represent the complex immediately before aminoacyl-tRNA synthesis (pre-aminoacyl-tRNA synthesis step) and the AMP-bound PylRS structures represent the complex immediately after aminoacyl-tRNA synthesis (post-aminoacyl-tRNA synthesis step) (Fig. 6). Furthermore, crystallographic analyses of the various PylRS structures revealed that the large structural changes of the functionally essential Asn346 side chain, which hydrogen-bonds to the N^{ε}-carbonyl group of the amino-acid substrate, may be relevant to the aminoacyl-tRNA synthesis reaction, as discussed below. On the other hand, the conformational changes of the motif 2 and ordering loops are induced upon binding the adenylate moiety of ATP and those of the $\beta7$–$\beta8$ hairpin occur regardless of substrate binding, as described previously (Yanagisawa *et al.*, 2008*a*). To avoid steric hindrance with the tRNA acceptor stem, the $\beta7$–$\beta8$ hairpin adopts an open conformation when tRNA enters the active site of PylRS (Fig. 6; Yanagisawa *et al.*, 2008*a*; Nozawa *et al.*, 2009).

To date, 13 crystal structures of *M. mazei* PylRS(c270), including the ligand-free and several ligand-bound forms, have been solved (Table 1). A comparison of these structures revealed conformational changes of the side-chain amide group of Asn346 which are essential for PylRS activity (Fig. 6; Yanagisawa *et al.*, 2008*a*). In general, PylRS exhibits higher affinity for ATP than amino-acid substrates (the K_m values for ATP and Pyl are 2 and 50 μM, respectively; Blight *et al.*, 2004; Polycarpo *et al.*, 2006). The bound ATP molecule stabilizes the PylRS active site and might form part of the binding site for the amino-acid substrate. The side-chain amide group of Asn346 points toward the ATP (or AMPPNP) binding site in the ligand-free state (Yanagisawa *et al.*, 2008*a*) and in the post-aminoacyl-tRNA synthesis step (the present AMP-bound form). In the ATP-binding step (the AMPPNP-bound form), the side chain of Asn346 points in both directions. It points toward the AMPPNP phosphate in the structure reported by Kavran *et al.* (2007), while the electron density of the Asn346 was dispersed in our previously reported structure (Yanagisawa *et al.*, 2008*a*). The Asn346 side chain fluctuates by approximately 60° during ATP binding. On the other hand, in the structures representing the fixed state of amino-acid binding [CpocLys–ATP-bound (Kavran *et al.*, 2007), Pyl–AMPPNP-bound (Yanagisawa *et al.*, 2008*a*) and form 1 (Yanagisawa *et al.*, 2008*a*)] and the step after aminoacyl-AMP synthesis (Pyl-AMP-bound; Kavran *et al.*, 2007) the amide N atom of the Asn346 side chain hydrogen-bonds to the N^{ε}-carbonyl group of the amino-acid substrate and the amide O atom of the Asn346 side chain interacts with the α-amino or α-carboxyl group of the amino-acid substrate by a water-mediated hydrogen-bond interaction (Fig. 3*e*). In the pre-aminoacyl-tRNA synthesis step (the BocLys-AMP-bound form), the side-chain amide group of Asn346 points toward the amino-acid substrate and hydrogen bonds to the N^{ε}-carbonyl group of BocLys. However, there are no hydrogen bonds between Asn346 and the α-amino group of BocLys owing to the absence of water-mediated interactions. The Asn346 side chain shifts its direction by a maximum of 85–90° around the C^{β} atom of Asn346 compared with its orientation in the Pyl-AMP-bound/Pyl–AMPPNP-bound and ligand-free forms (Fig. 6). The present structures of PylRS in a novel crystal form have revealed the pre- and post-aminoacyl-tRNA synthesis conformational states of the adenylate and aminoacyl moieties and the orientation of the asparagine residue in the catalytic site. The present structures may correspond to the last step of adenylate formation (the pre-aminoacyl-tRNA synthesis stage) and a step after the release of the aminoacyl-tRNA from PylRS prior to AMP release, which would generate the free enzyme ready for another cycle of aminoacylation (the post-aminoacyl-tRNA synthesis stage).

All of the previously determined structures of *M. mazei* PylRS belonged to the hexagonal crystal family, whereas the present AMP-bound and BocLys-AMP-bound structure of *M. mazei* PylRS belongs to the triclinic crystal family. Crystal polymorphs for capturing different conformational states have been well studied for the tryptophanyl-tRNA synthetases (TrpRSs; Retailleau *et al.*, 2003, 2007; Buddha & Crane, 2005; Shen *et al.*, 2008; Zhou *et al.*, 2010) and tyrosyl-tRNA synthetases (TyrRSs; Kobayashi *et al.*, 2005; Zhang *et al.*, 2005). In *Bacillus stearothermophilus* TrpRS (bTrpRS), TrpRS

ligands induce large-scale conformational changes in the bTrpRS structures from the open state (ligand-free form) to the closed pre-transition state (Trp- and ATP-bound form) and the closed product state (Trp-AMP-bound form) (Retailleau *et al.*, 2003, 2007). Crystals of the open state of bTrpRS belong to the monoclinic and triclinic crystal families, while those of the closed pre-transition and closed product states of bTrpRS belong to the tetragonal crystal family. On the other hand, local but not large-scale conformational changes upon substrate binding have been observed in TyrRS (Kobayashi *et al.*, 2005). Likewise, many cases that have captured different conformations of other aaRSs upon binding of aaRS ligands or in ligand-free forms have been reported (Cusack *et al.*, 1996, 2000; Schmitt *et al.*, 1998; Eiler *et al.*, 1999; Rees *et al.*, 2000; Onesti *et al.*, 2000; Sauter *et al.*, 2000; Delagoutte *et al.*, 2000; Yaremchuk *et al.*, 2001; Sekine *et al.*, 2003; Crepin *et al.*, 2003; Torres-Larios *et al.*, 2003; Swairjo & Schimmel, 2005; Moor *et al.*, 2006; Bilokapic *et al.*, 2008; Yanagisawa *et al.*, 2008*a*). Among these, however, there were no cases that captured the aaRS structures of the AMP-bound (the post-aminoacyl-tRNA synthesis stage) and aminoacyl-AMP-bound (the pre-aminoacyl-tRNA synthesis stage) forms in a single crystal, and no similar crystallization methods that shed light on the mechanistics of aaRSs have been reported for the other aaRSs. This is the first report of crystal polymorphs for capturing the conformational states in the *M. mazei* PylRS structures. Crystal polymorphs grown under various buffer conditions can capture different conformational states and this technique may be useful to study the structural dynamics of aaRSs.

We would like to thank the staff of beamline BL41XU at SPring-8 (Harima, Japan) as well as the staff of the BL-5A and AR-NW12 beamlines at the Photon Factory (Tsukuba, Japan). We also thank Drs Shun-ichi Sekine, Takuhiro Ito, Ryuya Fukunaga (The University of Tokyo) and Toru Sengoku (RIKEN) for assisting with the data collection and for helpful discussions. We would like to thank Azusa Ishii and Tomoko Nakayama for clerical assistance. This work was supported in part by Grants-in-Aid for Scientific Research from the Ministry of Education, Culture, Sports, Science and Technology (MEXT) of Japan, the RIKEN Structural Genomics/Proteomics Initiative (RSGI) in the National Project on Protein Structural and Functional Analyses, MEXT and the Targeted Proteins Research Program (TPRP), MEXT.

References

Aberg, A., Yaremchuk, A., Tukalo, M., Rasmussen, B. & Cusack, S. (1997). *Biochemistry*, **18**, 3084–3094.

Arnez, J. G., Dock-Bregeon, A. C. & Moras, D. (1999). *J. Mol. Biol.* **286**, 1449–1459.

Arnez, J. G., Harris, D. C., Mitschler, A., Rees, B., Francklyn, C. S. & Moras, D. (1995). *EMBO J.* **14**, 4143–4155.

Belrhali, H., Yaremchuk, A., Tukalo, M., Larsen, K., Berthet-Colominas, C., Leberman, R., Beijer, B., Sproat, B., Als-Nielsen, J., Grübel, G., Legrand, J.-F., Lehmann, M. & Cusack, S. (1994). *Science*, **263**, 1432–1436.

Bilokapic, S., Maier, T., Ahel, D., Gruic Sovulj, I., Söll, D., Weygand-Durasevic, I. & Ban, N. (2006). *EMBO J.* **25**, 2498–2509.

Bilokapic, S., Rokov Plavec, J., Ban, N. & Weygand-Durasevic, I. (2008). *FEBS J.* **275**, 2831–2844.

Blight, S. K., Larue, R. C., Mahapatra, A., Longstaff, D. G., Chang, E., Zhao, G., Kang, P. T., Green-Church, K. B., Chan, M. K. & Krzycki, J. A. (2004). *Nature (London)*, **431**, 333–335.

Bovee, M. L., Pierce, M. A. & Francklyn, C. S. (2003). *Biochemistry*, **42**, 15102–15113.

Brünger, A. T., Adams, P. D., Clore, G. M., DeLano, W. L., Gros, P., Grosse-Kunstleve, R. W., Jiang, J.-S., Kuszewski, J., Nilges, M., Pannu, N. S., Read, R. J., Rice, L. M., Simonson, T. & Warren, G. L. (1998). *Acta Cryst.* D**54**, 905–921.

Buddha, M. R. & Crane, B. R. (2005). *J. Biol. Chem.* **280**, 31965–31973.

Cavarelli, J., Eriani, G., Rees, B., Ruff, M., Boeglin, M., Mitschler, A., Martin, F., Gangloff, J., Thierry, J.-C. & Moras, D. (1994). *EMBO J.* **13**, 327–337.

Crepin, T., Schmitt, E., Mechulam, Y., Sampson, P. B., Vaughan, M. D., Honek, J. F. & Blanquet, S. (2003). *J. Mol. Biol.* **332**, 59–72.

Cusack, S., Berthet-Colominas, C., Härtlein, M., Nassar, N. & Leberman, R. (1990). *Nature (London)*, **347**, 249–255.

Cusack, S., Yaremchuk, A. & Tukalo, M. (1996). *EMBO J.* **15**, 2834–2842.

Cusack, S., Yaremchuk, A. & Tukalo, M. (2000). *EMBO J.* **19**, 2351–2361.

Delagoutte, B., Moras, D. & Cavarelli, J. (2000). *EMBO J.* **19**, 5599–5610.

Eiler, S., Dock-Bregeon, A., Moulinier, L., Thierry, J.-C. & Moras, D. (1999). *EMBO J.* **18**, 6532–6541.

Emsley, P. & Cowtan, K. (2004). *Acta Cryst.* D**60**, 2126–2132.

Eriani, G., Delarue, M., Poch, O., Gangloff, J. & Moras, D. (1990). *Nature (London)*, **347**, 203–206.

Hao, B., Gong, W., Ferguson, T. K., James, C. M., Krzycki, J. A. & Chan, M. K. (2002). *Science*, **296**, 1462–1466.

Ibba, M. & Söll, D. (2000). *Annu. Rev. Biochem.* **69**, 617–650.

Jones, T. A., Zou, J.-Y., Cowan, S. W. & Kjeldgaard, M. (1991). *Acta Cryst.* A**47**, 110–119.

Kavran, J. M., Gundllapalli, S., O'Donoghue, P., Englert, M., Söll, D. & Steitz, T. A. (2007). *Proc. Natl Acad. Sci. USA*, **104**, 11268–11273.

Kobayashi, T., Takimura, T., Sekine, R., Kelly, V. P., Vincent, K., Kamata, K., Sakamoto, K., Nishimura, S. & Yokoyama, S. (2005). *J. Mol. Biol.* **346**, 105–117.

Krissinel, E. & Henrick, K. (2004). *Acta Cryst.* D**60**, 2256–2268.

Lee, M. M., Jiang, R., Jain, R., Larue, R. C., Krzycki, J. & Chan, M. K. (2008). *Biochem. Biophys. Res. Commun.* **374**, 470–474.

Moor, N., Kotik-Kogan, O., Tworowski, D., Sukhanova, M. & Safro, M. (2006). *Biochemistry*, **45**, 10572–10583.

Murshudov, G. N., Skubák, P., Lebedev, A. A., Pannu, N. S., Steiner, R. A., Nicholls, R. A., Winn, M. D., Long, F. & Vagin, A. A. (2011). *Acta Cryst.* D**67**, 355–367.

Nozawa, K., O'Donoghue, P., Gundllapalli, S., Araiso, Y., Ishitani, R., Umehara, T., Söll, D. & Nureki, O. (2009). *Nature (London)*, **457**, 1163–1167.

Onesti, S., Desogus, G., Brevet, A., Chen, J., Plateau, P., Blanquet, S. & Brick, P. (2000). *Biochemistry*, **39**, 12853–12861.

Otwinowski, Z. & Minor, W. (1997). *Methods Enzymol.* **276**, 307–326.

Polycarpo, C., Ambrogelly, A., Bérubé, A., Winbush, S. M., McCloskey, J. A., Crain, P. F., Wood, J. L. & Söll, D. (2004). *Proc. Natl Acad. Sci. USA*, **101**, 12450–12454.

Polycarpo, C. R., Herring, S., Bérubé, A., Wood, J. L., Söll, D. & Ambrogelly, A. (2006). *FEBS Lett.* **580**, 6695–6700.

Rees, B., Webster, G., Delarue, M., Boeglin, M. & Moras, D. (2000). *J. Mol. Biol.* **299**, 1157–1164.

Retailleau, P., Huang, X., Yin, Y., Hu, M., Weinreb, V., Vachette, P., Vonrhein, C., Bricogne, G., Roversi, P., Ilyin, V. & Carter, C. W. (2003). *J. Mol. Biol.* **325**, 39–63.

Retailleau, P., Weinreb, V., Hu, M. & Carter, C. W. (2007). *J. Mol. Biol.* **369**, 108–128.
Ruff, M., Krishnaswamy, S., Boeglin, M., Poterszman, A., Mitschler, A., Podjarny, A., Rees, B., Thierry, J.-C. & Moras, D. (1991). *Science*, **252**, 1682–1689.
Sauter, C., Lorber, B., Cavarelli, J., Moras, D. & Giegé, R. (2000). *J. Mol. Biol.* **299**, 1313–1324.
Schimmel, P. (1987). *Annu. Rev. Biochem.* **56**, 125–158.
Schmitt, E., Moulinier, L., Fujiwara, S., Imanaka, T., Thierry, J.-C. & Moras, D. (1998). *EMBO J.* **17**, 5227–5237.
Sekine, S., Nureki, O., Dubois, D. Y., Bernier, S., Chênevert, R., Lapointe, J., Vassylyev, D. G. & Yokoyama, S. (2003). *EMBO J.* **22**, 676–688.
Shen, N., Zhou, M., Yang, B., Yu, Y., Dong, X. & Ding, J. (2008). *Nucleic Acids Res.* **36**, 1288–1299.
Srinivasan, G., James, C. M. & Krzycki, J. A. (2002). *Science*, **296**, 1459–1462.
Swairjo, M. A. & Schimmel, P. R. (2005). *Proc. Natl Acad. Sci. USA*, **102**, 988–993.
Takimoto, J. K., Dellas, N., Noel, J. P. & Wang, L. (2011). *ACS Chem. Biol.* **6**, 733–743.
Torres-Larios, A., Sankaranarayanan, R., Rees, B., Dock-Bregeon, A. C. & Moras, D. (2003). *J. Mol. Biol.* **331**, 201–211.
Winn, M. D. *et al.* (2011). *Acta Cryst.* D**67**, 235–242.
Yanagisawa, T., Ishii, R., Fukunaga, R., Kobayashi, T., Sakamoto, K. & Yokoyama, S. (2008*a*). *J. Mol. Biol.* **378**, 634–652.
Yanagisawa, T., Ishii, R., Fukunaga, R., Kobayashi, T., Sakamoto, K. & Yokoyama, S. (2008*b*). *Chem. Biol.* **15**, 1187–1197.
Yanagisawa, T., Ishii, R., Fukunaga, R., Nureki, O. & Yokoyama, S. (2006). *Acta Cryst.* F**62**, 1031–1033.
Yaremchuk, A., Tukalo, M., Grøtli, M. & Cusack, S. (2001). *J. Mol. Biol.* **309**, 989–1002.
Zhang, Y., Wang, L., Schultz, P. G. & Wilson, I. A. (2005). *Protein Sci.* **14**, 1340–1349.
Zhou, M., Dong, X., Shen, N., Zhong, C. & Ding, J. (2010). *Nucleic Acids Res.* **38**, 3399–3413.